Microfluidics and Nanofluidics (2022) 26:101
https://doi.org/10.1007/s10404-022-02605-4

RESEARCH PAPER

# Fluid transportation by droplets impacting wettability-controlled surfaces at the nanoscale: a molecular dynamics simulation study

Ya-Nan Dong[1] · Ning-Ning Han[2] · Xing-Juan Zhang[3] · Ben-Xi Zhang[4,5] · Jun-Yao Wang[3] · Xin He[3]

Received: 22 April 2022 / Accepted: 20 October 2022 / Published online: 8 November 2022


## Abstract

This work investigates nanodroplets impacting wettability-controlled surfaces via MD simulations. In comparison with fluid transportation of droplets at the macroscale, which is effective on hydrophilic/superhydrophobic surfaces, the one at the nanoscale is only achieved for nanodroplets on hydrophobic/hydrophobic or hydrophobic/superhydrophobic surfaces. This difference lies in the different transportation mechanism that breakup can take place for the former with the part on the superhydrophobic side being tossed, whereas, the droplets in the latter process always forms as an intact one owing to the enhanced viscous force at the nanoscale, indicating the transportation by bouncing instead of tossing. More quantitatively, the normalized transportation velocity, $V^* = V_t/V_0$, is extracted from MD simulation results, where $V_t$ is the transportation velocity and $V_0$ is the impact velocity. This feature parameter is controlled by the difference of contact angles ($\Delta\theta$) and impact velocity and our simulations show two kinds of conditions are found to have a good performance of fluid transportation at the nanoscale, i.e., high $V_0$ with high $\Delta\theta$ and low $V_0$ with $\Delta\theta$. Finally, a simple energy conversion model with a fitting parameter is established for quantifying the relationship between $V^*$ and $\Delta\theta$, attesting that the mechanism of fluid transportation at the nanoscale stems from the difference surface energy of the liquid–gas interface on wettability-controlled surfaces.

**Keywords** Nanodroplet impact · Molecular dynamics simulation · Fluid transportation · Wettability-controlled surface

## 1 Introduction

The phenomenon of a droplet impacting a surface is ubiquitous not only in natural life, for example, rain droplets impacting solid surfaces, but also in industrial processes, such as aircraft icing (Mishchenko et al. 2010), water harvesting (Wang et al. 2019a) and so forth (Wang et al. 2022). After impacting surfaces, droplets have rich outcomes, such as spreading, retraction, sticky, splashing, break-up, and bouncing (Josserand and Thoroddsen 2016). Among these outcomes, bouncing reached increasing attention owing to its potential in many applications, such as the design of anti-icing (Kreder et al. 2016) and self-clean surfaces (Hassan et al. 2020), the control of droplets (Hao et al. 2018), and so forth. Many studies have been devoted to revealing the mechanism of bouncing droplets via experiments (Bertola 2009; Bird et al. 2013; Caviezel et al. 2008; Chantelot et al. 2018; Chen and Li 2010; Gilet and Bush 2012; Gomaa et al. 2020; Hao et al. 2015; Jung and Bhushan 2008; Liu et al. 2014; Okumura et al. 2003; Richard et al. 2002; Richard and Quéré 2000; Wang et al. 2019b), numerical simulations (Caviezel et al. 2008; Xie et al. 2020), and theoretical analysis (Chantelot et al. 2018; Okumura et al. 2003; Richard et al. 2002; Richard and Quéré 2000; Xie et al. 2020).

At the macroscale, the contact time is one of the most concerned parameters which has been investigated in two decades. Richard et al. (2002) first reported

✉ Jun-Yao Wang
junyao_0001@126.com

✉ Xin He
66921009@qq.com

1 ChangChun Education Institute, Changchun 130052, China

2 Key Laboratory of Condition Monitoring and Control for Power Plant Equipment, North China Electric Power University, Beijing 102206, China

3 Department of Mechanical Engineering, Northeast Electric Power University, Jilin 132000, China

4 State Key Laboratory of Alternate Electrical Power System with Renewable Energy Sources, North China Electric Power University, Beijing 102206, China

5 School of Mechanical Engineering, Northeast Electric Power University, JiLin 132000, China

a breakthrough by proposing a scaling law of the contact time, i.e., $\tau_c \sim We^{1/2}R_0/V_0$ with the prefactor of 2.6, where $We(=\rho D_0 V_0^2/\gamma)$ is the Weber number representing the ratio of inertial to capillary forces, $\tau_c$ is the contact time, $\rho$ is the density of liquids, $R_0$ is the radius of impacting droplet, $V_0$ is the impact velocity, and $\gamma$ is the surface tension of liquids. They indicated that viscosity is not important in the bouncing of low-viscosity droplets. Bird et al. (2013) collected data on the contact time of droplets impacting hydrophobic or superhydrophobic surfaces and further confirmed the scaling law. Subsequently, they indicated that there exist experimental and theoretical limits to the contact time of bouncing droplets. In experiments, no matter how superhydrophobic the surface is, even the contact angle approaching 180°, the prefactor of the scaling law could not be lower than 2.6; furthermore, despite viscous effects being neglected by considering the impact of droplets as a perfectly elastic collision, the prefactor is limited to 2.2. For further reducing the contact time, Bird et al. (2013) decorated a surface with a rigid for inducing non-axisymmetric retraction of impacting droplets, successfully achieving the significant reduction by 37% in comparison with the contact time on regular surfaces. Following this work, many kinds of structures are decorated to surfaces for reducing the contact time, such as a point-like superhydrophobic macrotexture (Chantelot et al. 2018), submillimetre-scale posts (Liu et al. 2014), and so forth.

Recently, Chu et al. (2020) discussed the later process of droplets bouncing off surfaces and indicated that if the superhydrophobic surface is horizontally located, no matter how short the contact time is, the bouncing droplet would finally fall back to the surface owing to the action of gravity. Therefore, in comparison with the reduction of the contact time, a directional transportation of droplets has a practical requirement and is more expected. Hao et al. (2018) proposed a droplet jumping intensification device and reported that the droplet trajectory can be controlled by the droplet size, impact Weber number, and the height of the mini-channel of the device. Despite the good performance of this device on fluid transportation, however, the device is closed, which limits the application condition of this device, especially, the design of anti-icing surfaces. In this context, adopting a wettability-controlled surface can be considered an alternative choice. Schutzius et al. (2014) proposed a hydrophobic surface with arc-shaped and hydrophilic parts to control the motion of impacting droplets. In comparison with surfaces decorated by ridges, the droplet on wettability-controlled surfaces can bounce with lateral velocity, indicating that fluid transportation is successfully achieved. Similarly, Chu et al. (2020) reported a wettability-controlled surface with half part being superhydrophobic and the other part being hydrophilic can induce the directional transportation of impacting droplets. On this wettability-controlled surface, non-asymmetric retraction occurs for proving the lateral bouncing velocity, and the maximum transportation distance can be larger than ten times the droplet diameter.

The dynamics of impacting nanodroplets reached increasing attention nowadays because not only it is common in natural life, for example, suspended water droplets in foggy days, but also it is potential in many promising applications, such as nanoscale inkjet printing (Galliker et al. 2012), producing high-entropy materials (Glasscott et al. 2019), and so forth. Unfortunately, the investigation of nanodroplets is challenging work. First, the direct observation of dynamic processes of impacting nanodroplets is almost impossible to implement owing to the limited performance of high-speed cameras. Besides, traditional numerical simulation methods, for example, computational fluid mechanics (CFD) are difficult to investigate the dynamics of nanodroplets accurately unless the properties of fluids are modified or complex boundary conditions are adopted (Garajeu et al. 2013). In this context, the molecular dynamics (MD) method is an atom-based method that simulates the dynamics of nanodroplets by tracing the path of each atom, and hence, MD simulations have natural advantages in exploring the dynamic mechanism of nanodroplets. Up to now, MD simulations have become one of the most effective tools in the dynamics of nanodroplets, such as droplet coalescence at the nanoscale (Pak et al. 2018; Xie et al. 2018a, b), wetting transition in nanostructures (Zhang et al. 2019, 2021), and so forth. In particular, the impact dynamics of nanodroplets have been investigated detailed in recent years by MD simulations and many novel mechanisms of nanodroplets have been revealed (Xie et al. 2020; Gao et al. 2018; Kobayashi et al. 2016; Koishi et al. 2017; Li et al. 2015, 2017; Sun et al. 2022; Wang et al. 2019c, 2020a, b). Li et al. (2015) examined water nanodroplets on surfaces with a contact angle of $\theta = 125°$ and indicated that the viscous dissipation mechanism is different from millimeter-sized droplets with the viscous dissipation occurring in entire nanodroplets instead of concentrates in the boundary layer. Here, $\theta$ represents the static contact angle, determined by the contact angle of an equilibrium droplet at the three-phase contact line. Therefore, the viscous effect at the nanoscale is more significant. This conclusion is attested by the following studies. For example, Xie et al. (2020) examined Ar nanodroplets on superhydrophobic surfaces with $\theta = 150°$ and indicated that instead of $\tau_c \sim We^{1/2}R_0/V_0$ the scaling law of the contact time at the nanoscale is $\tau_c \sim Re^{-1/3}We^{2/3}R_0/V_0$, where $Re(=\rho D_0 V_0/\mu)$ is the Reynolds number representing the ratio of inertial to viscous forces and $\mu$ is the viscosity of liquids. The effect of Re in the scaling law of nanodroplets further proved the important role of viscous force at the nanoscale. In addition to enhanced viscous force at the nanoscale, impacting nanodroplets were found more sensitive to surface wettability in comparison with millimeter-sized droplets. Wang et al.

(2020a) examined water nanodroplets on surfaces with $\theta$ from 23° to 148° and indicated that the velocity of the contact line of nanodroplets in spreading is significantly affected by surface wettability, i.e., on a more hydrophilic surface, a faster moving velocity of nanodroplets would occur and further reach a larger maximum spreading diameter.

Despite progress in impact dynamics of nanodroplets on homogeneous surfaces, there is a lack of investigations of controlling droplets in fluid transportation, and especially, whether the proposed surfaces for millimeter-sized droplets are still effective for nanodroplets is required to be further attested. Owing to the significant performance of fluid transportation on wettability-controlled surfaces proposed by Chu et al. (2020), we adopted similar surfaces, i.e., the wettability of the half-one surface is lower than the other half-one.

This work aims for revealing the mechanism of fluid transportation at the nanoscale and subsequently uncovering the difference of transportation mechanisms at the nanoscale and the macroscale. Then, based on MD simulations, which kinds of surface features of wettability-controlled surface can have good performance is desired to be identified. Finally, a simple model is expected to be obtained to quantify the relationship between the transportation performance and the surface feature of wettability-controlled surfaces.

## 2 Simulation methods

In this paper, MD simulations are implemented to investigate the impact dynamics of nanodroplets on wettability-controlled surfaces. All simulations are conducted using the LAMMPS (large-scale atomic/molecular massively parallel simulator) package. The initial system is shown in Fig. 1a, the red atom is the mW atom and each mW atom represents a water molecule by the mW model (which will be discussed later) with $Mr_{mW}$ of 18 g mol$^{-1}$; The blue and yellow atoms are all the solid atoms $Mr_{soild}$ of 195 g mol$^{-1}$, where Mr represents the relative molecular mass. The simulation system has a diameter of $48\times48\times28$ nm$^3$ with a water nanodroplet and a solid substrate. The water nanodroplet has a diameter of 10 nm and consists of 17,528 mW atoms. The periodic boundary condition is applied to all three directions. The water nanodroplet and solid substrate are produced using centered cubic crystals with the help of the density of water and solid at the temperature of 300 K. The solid substrate has seven layers of atoms with the bottom three layers being fixed and the other layers being free. All solid atoms are applied with a virtual spring to their initial position for preventing the deformation of the solid substrate during impact. It is worth noting that left- or right-side solid has different surface wettability for producing a wettability-controlled surface with contact angle $\theta_1$ or $\theta_2$, respectively. Here, $\theta_1$ is always lower than $\theta_2$ and the difference of contact angles, $\Delta\theta$, is defined as $\theta_2$–$\theta_1$.

The interaction between water molecules (w–w) is implemented by the monatomic water (mW) model. The mW model was developed by Molinero and Moore (2009), which is derived from the Stillinger–Weber potential model of silicon on the basis of the monatomic short-range multibody potential. In comparison with the TIP4P and SPC/E models, the mW model is a coarse-graining model, which considers a water molecule as a coarse-grained atom, and thereby can significantly reduce the computational cost. Nonetheless, despite being a coarse-graining model, the mW model can accurately reproduce the physical properties of water, such as density, surface tension and so forth. This model has been widely used in the investigation of the impact dynamics of nanodroplets. According to MD simulations from previous works, the density, surface tension, and viscosity of water modeled by the mW model are $\rho=996$ kg/m$^3$, $\gamma=66$ mN m$^{-1}$, and $\mu=283.7$ μPa s (Molinero and Moore 2009; Jacobson et al. 2014; Moore and Molinero 2011).

The Lennard–Jones potential to model the interactions between water–solid (w–s) and solid–solid (s–s) is adopted and expressed as follows:

$$U_{LJ}(r)=4\varepsilon\left[\left(\frac{\sigma}{r}\right)^{12}-\left(\frac{\sigma}{r}\right)^{6}\right],\quad r<r_{cut} \tag{1}$$

where $\varepsilon$ is the depth of the potential well, $\sigma$ is the effective interaction distance, and the $r_{cut}$ is the cut-off distance, which is set as 1 nm. The interaction parameters of s–s and w–s are set as $\varepsilon_{s-s}=0.69375$ eV, $\sigma_{s-s}=0.247$ nm and $\sigma_{w-s}=0.28155$ nm (Li et al. 2015, 2017; Wang et al. 2020a, b; Ma et al. 2021), whereas, the potential parameter $\varepsilon_{w-s}$ is used to be an adjustable parameter to produce different surface wettability. Here, the relationship between the contact angle and potential parameter $\varepsilon_{w-s}$ has been investigated in detail in previous work. When the interaction parameter $\varepsilon_{w-s}$ equals 0.02, 0.01684, 0.0102, 0.0068, 0.0051 and 0.00184 eV, the contact angle is obtained as $\theta=55°$, 73°, 85°, 105°, 125°, 148°, and 180° (Wang et al. 2020a). The contact angle is measured by evaluating the angle at the three-phase triple line, which is widely used in many works.

After the simulation system and interactions of atoms are set, MD simulations can be implemented. In general, there are two processes for each case, i.e., the equilibrium process and the outcome process, and the time step is adopted as 1 fs. The equilibrium process runs in the NVT ensemble (canonical ensemble) with the Nose–Hoover thermostat being adopted to control the system temperature at 300 K. The center of mass of the nanodroplet is controlled away from the solid surface for avoiding the interaction between the nanodroplet and solid surface in the equilibrium process. This process takes 500,000 time steps. After the equilibrium

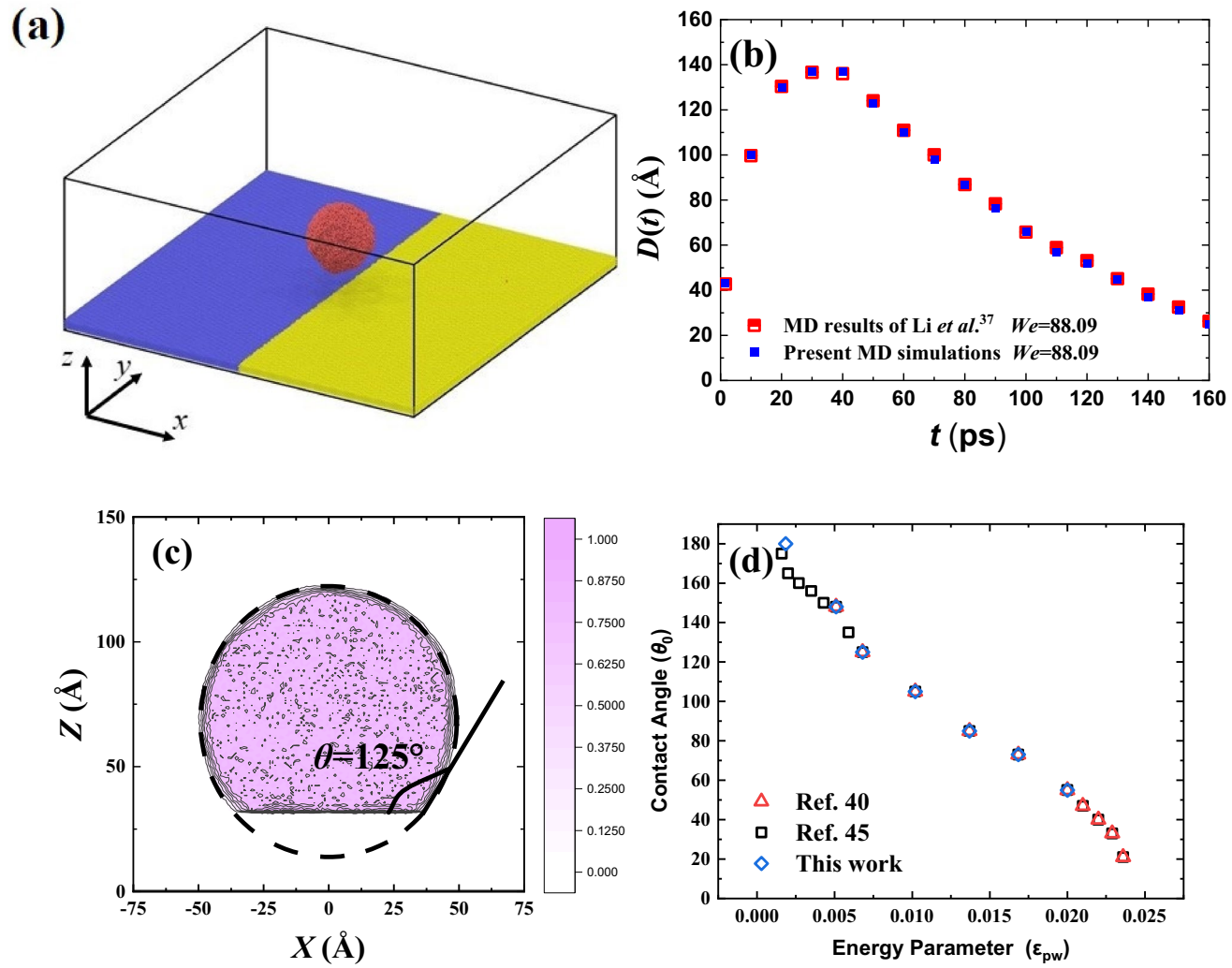


**Fig. 1** **a** A snapshot of the system which contains a nanodroplet over a wettability-controlled surface. The contact angle of the high-wettability side is $\theta_1$, which is lower than the one of the low-wettability side with $\theta_2$. **b** The density contours of a nanodroplet at $\varepsilon_{w-s}=0.0068$ eV. **c** The comparison of spreading diameter of results between this work and Li et al. (2015). **d** The comparison of contact angle with $\varepsilon_{water-Pt}$ interaction parameter between this work and Wang et al. (2020a) and Ma et al. (2021)

process, the outcome process is implemented in the NVE ensemble (micro-canonical ensemble). In this process, the Nose–Hoover thermostat and the control of the center of mass of the nanodroplet are removed. Besides, a velocity is given to the nanodroplet for driving the impact process. The position and velocity of each atom are recorded and stored every 1 ps for further analysis. The cases are calculated on Inter Xeon E5-2697 v4 processors and one case would take about 20 h on 36 threads.

For validating the accuracy of simulations in this work, the code of our simulations and the correctness between the contact angles and the $\varepsilon_{w-s}$ interaction parameters are validated below. The code is validated by comparing the spreading radius ($R$) from simulations by our code and the results from Li et al. (2015) at the same conditions, i.e., the same droplet diameter, the same impact velocity, and interaction parameters between atoms. As shown in Fig. 1b, our simulation results show good agreement with the ones from Li et al. (2015). Besides, for validating the correctness between the contact angles and the $\varepsilon_{w-s}$ interaction parameters listed above, the simulation of estimating the contact angle is also implemented. The process of estimating contact angle has two steps. The first step is the relaxation of a nanodroplet on a substrate. After the relaxation, the nanodroplet reaches the equilibrium state. Subsequently, in the second step, fitting the profile of the nanodroplet as a circle and estimating the angle at the three-phase contact line leads to the value of the contact angle. For example, as shown in Fig. 1c, the contact angle is measured as 125° when $\varepsilon_{w-s}=0.0068$ eV. Subsequently, the comprehensive comparison between the

contact angle measured in this work and the ones in Wang et al. (2020a) and Ma et al. (2021) is shown in Fig. 1d. The relationship between the contact angle and the $\varepsilon_{w-s}$ interaction parameter listed above is validated.

## 3 Results and discussion

### 3.1 Nanodroplets impacting hydrophilic/hydrophobic and hydrophilic/superhydrophobic surfaces

Nanodroplets impacting hydrophilic/hydrophobic and hydrophilic/superhydrophobic surfaces are exhibited in Fig. 2 with four surfaces with $\theta$ from 85°/105° to 85°/180° being examined. During spreading, the impacting nanodroplets gradually spread over the surfaces ($t = 7$ ps). Despite the different surface wettability at different sides, the nanodroplets almost reach the maximum spreading state at the same time of $t = 22$ ps. Besides, the maximum spreading diameter is almost the same on different surfaces at the maximum spreading state, which is attributed to the relatively strong inertial force in spreading in comparison with other forces (Wang et al. 2020a). At the end of the spreading process, the nanodroplets enter into retraction. At the early retraction stage ($t = 36$ ps), if $\Delta\theta$ is as low as 25° (Fig. 2a), the symmetry is not broken; whereas, as $\Delta\theta$ increases to be higher than 40° (Fig. 2b–d), the nanodroplet on the low-wettability ($\theta_2$) side has a significantly faster contact line velocity than that on the high-wettability ($\theta_1$) side. At the later stage of the retraction process ($t = 72$ ps), a significant difference in retraction on different sides is observed, i.e., the part of nanodroplet on the low-wettability side almost completed the retraction whereas the other part on high-wettability side still retracted. At the end of the retraction process, a nanodroplet would be lifted owing to the collision at the center of the nanodroplet. On hydrophobic/superhydrophobic surfaces, the lifting force can depart the part of nanodroplets on the low-wettability side from surfaces by overcoming the adhesion at $t = 72$ ps (Fig. 2c, d); whereas, owing to the relatively stronger adhesion between liquids and surfaces on hydrophilic surfaces, the other part of nanodroplets on the high-wettability side is pinned on surfaces. At $t = 140$ ps, the nanodroplet would move toward the hydrophilic side by

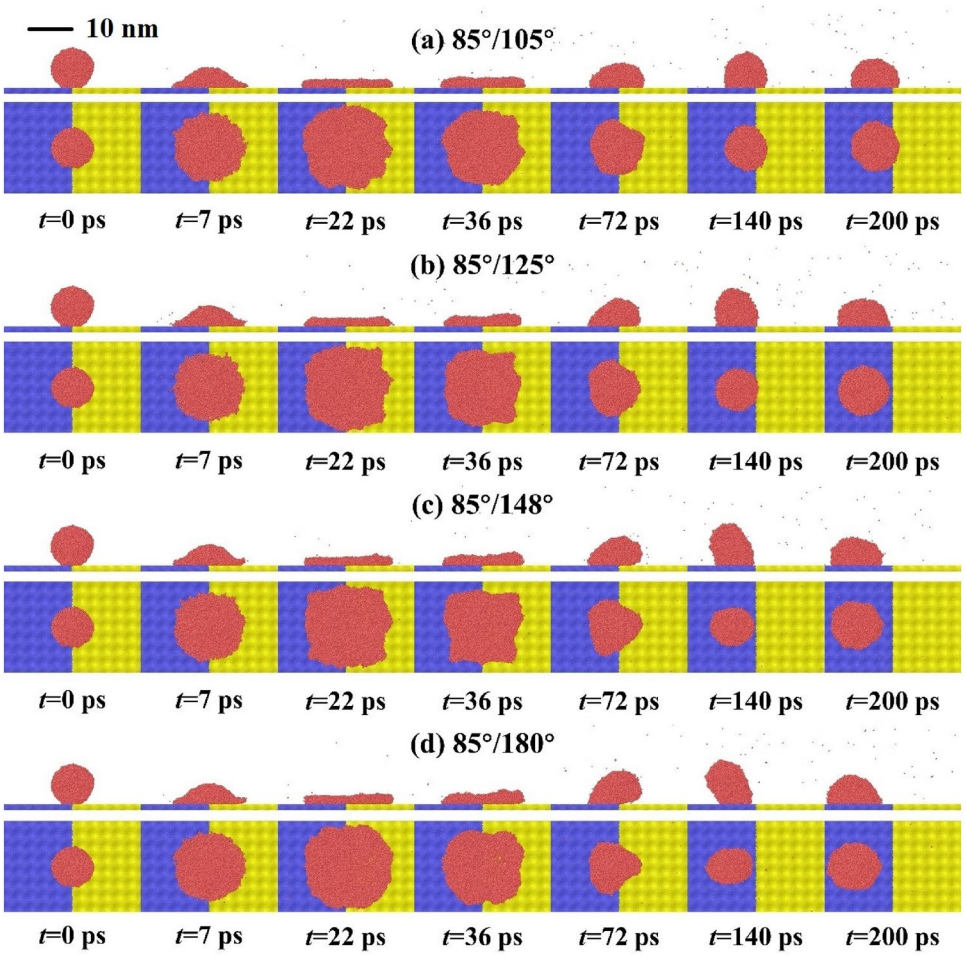


**Fig. 2** Snapshots of nanodroplets impacting surfaces with surface wettability from 85°/105° to 85°/180° at We = 84.89. Here, the scale bar presents 10 nm

the action of the unbalance capillary force on hydrophilic/hydrophobic surfaces ($\theta = 85°/105°$ and $\theta = 85°/125°$); whereas, the nanodroplet on hydrophilic/superhydrophobic surfaces shows the part of nanodroplet off surfaces is tossed toward to the hydrophilic side. Here needs to be noted that, for millimeter-sized droplets, a breakup can take place and the part of lifted liquids off surfaces can depart from the bulk of nanodroplets for achieving long-distance fluid transportation. However, despite the tossing process at the nanoscale, the breakup does not occur owing to enhanced viscous force at the nanoscale so that the tossed liquid part can not depart from the bulk of nanodroplet, indicating the failure of fluid transportation. At the end ($t = 200$ ps), nanodroplets are finally sticky on surfaces, no matter hydrophilic/hydrophobic or hydrophilic/superhydrophobic.

It is worth noting that, the breakup between pinned and tossed parts of nanodroplets does not take place but a new outcome is observed at the nanoscale as shown in Fig. 3, which is named as internal-breakup tossing. The spreading process is similar to snapshots in Fig. 2, however, when the nanodroplet starts to retract, an internal breakup occurs and a hole takes place at the low-wettability side at $t = 37$ ps. Subsequently, the hole is refilled by retracting liquid film at $t = 72$ ps and finally, the nanodroplet is sticky on surfaces as well. Due to the released surface energy from the maximum spreading state on the superhydrophobic side, the liquids on the superhydrophobic side are lifted and tossed during retraction. However, the released surface energy is not enough to lift liquids on the hydrophilic side. After reaching the maximum tossing state ($t = 141$ ps), the nanodroplet gradually reforms to a spherical-like shape ($t = 200$ ps) because of the action of surface tension. It is worth restating that, at the macroscale, fluid transportation is successfully achieved by the occurrence of a breakup to toss a part from the bulk droplet; however, at the nanoscale, the breakup is not observed, leading to the failure of the traditional fluid transportation mechanism. In this context, owing to the challenge of breakup at the nanoscale, bouncing droplets are desired to be effective at the nanoscale, but unfortunately, in our simulation cases for nanodroplets impacting on surfaces in the $\theta_2$ range from 105° to 180° with fixed $\theta_1 = 85°$ in a wide We range from 1.51 to 109.03, no bouncing is observed, indicating the failure of fluid transportation by bouncing on hydrophilic/hydrophobic or hydrophilic/superhydrophobic surfaces as well. Therefore, hydrophobic/hydrophobic and hydrophobic/superhydrophobic surfaces, which provide the possibility of bouncing, are expected to be more effective in fluid transportation at the nanoscale.

### 3.2 Nanodroplets impacting hydrophobic/hydrophobic and hydrophobic/superhydrophobic surfaces

Nanodroplets impacting hydrophobic/hydrophobic and hydrophobic/superhydrophobic surfaces are expected to have the capability of fluid transportation. It is worth noting beforehand that, there is a contradiction on fluid transportation by bouncing droplets because a more hydrophobic surface can lead droplets to bounce easily, however, this would result in a lower $\Delta\theta$, which would result in lower transportation performance. To identify what kinds of conditions can have good performance of fluid transportation, the impacts of nanodroplets on a wide range of wettability-controlled surfaces are examined. In this section, snapshots are exhibited first for making a comparison with impact processes on hydrophilic/hydrophobic or hydrophilic/superhydrophobic surfaces. Then the phase diagram of outcomes would be plotted for examining which cases have the outcome of bouncing, and finally, the transportation velocity, $V_t$, of these bouncing nanodroplets is extracted for exploring the conditions on a good performance of fluid transportation.

Snapshots are exhibited in Figs. 4, 5 and 6 with three series of wettability-controlled surfaces that the contact angles of the high-wettability side are 105°, 125°, and 148°, respectively. As shown in Fig. 4a, b, similar to that, despite a trend of tossing liquids, which is similar to the ones on hydrophilic/hydrophobic and hydrophilic/superhydrophobic surfaces, fluid transportation is not achieved owing to the absence of breakup. As $\Delta\theta$ increases (Fig. 4c), the nanodroplet can bounce off the surface with a significant lateral motion. As reported by Ma et al. (2021), a nanodroplet could not bounce from a homogeneity surface with $\theta$ being lower than 110°, however, on the wettability-controlled surface with $\theta = 105°/180°$, the nanodroplet successfully bounce from the surface with the help of provided energy from the low-wettability side. When nanodroplets impact surfaces with increased $\theta_1$, as exhibited in Figs. 5 and 6, due to the higher contact

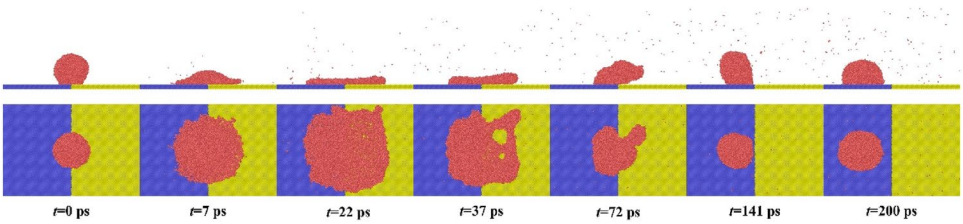


**Fig. 3** Snapshots of nanodroplets impacting surfaces with $\theta = 85°/180°$ at We = 109.03

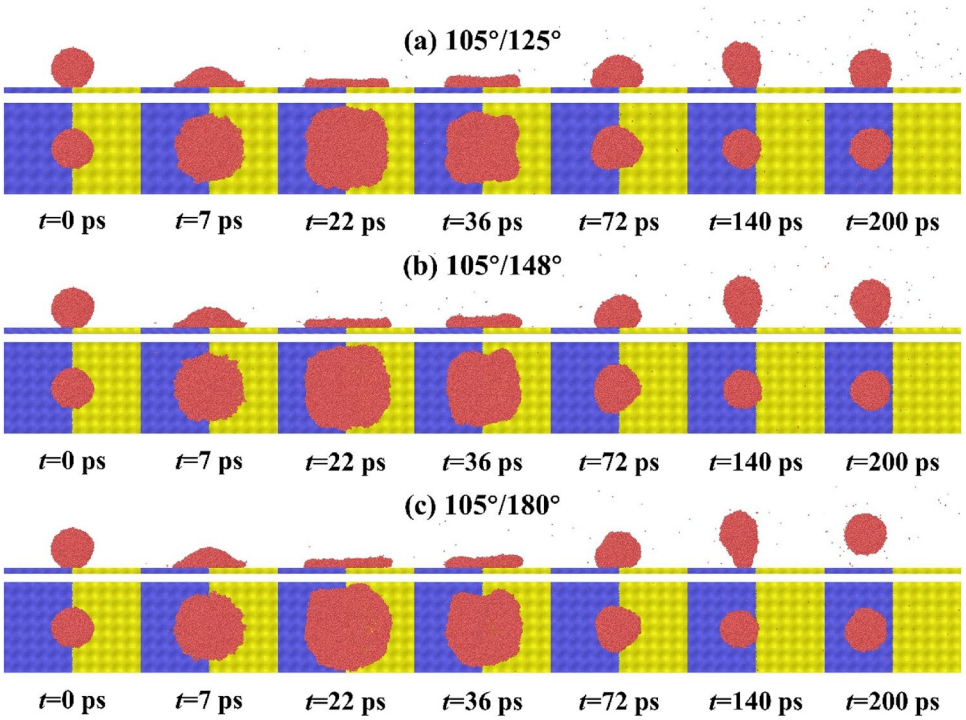


**Fig. 4** Snapshots of nanodroplets impacting surfaces with surface wettability from 105°/125° to 105°/180° at We = 84.89

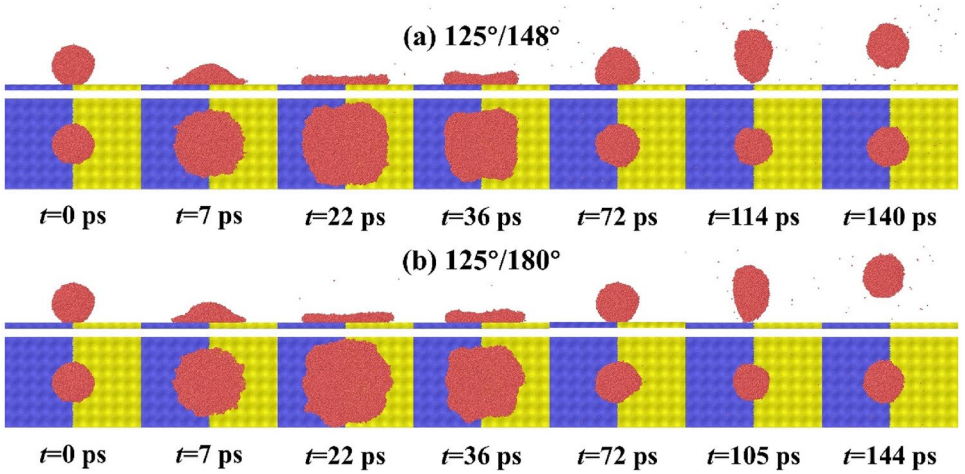


**Fig. 5** Snapshots of nanodroplets impacting surfaces with surface wettability from 125°/148° to 125°/180° at We = 84.89

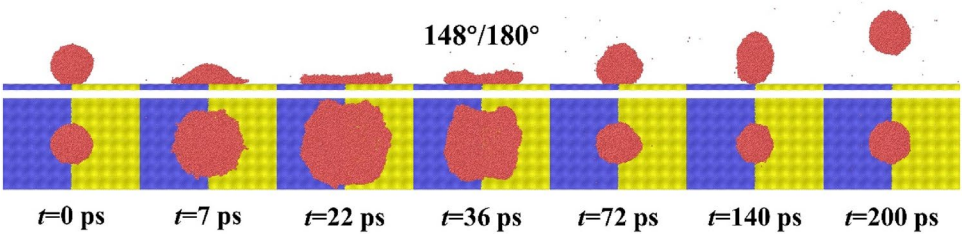


**Fig. 6** Snapshots of nanodroplets impacting surfaces with surface wettability of $\theta = 148°/180°$ at We = 84.89

angles, the nanodroplets are easier to bounce, however, the lateral motion is significantly reduced so that despite the occurrence of bouncing droplets, the fluid transportation is extremely inefficiency.

### 3.3 The criterion of bouncing

At the nanoscale, the fluid transportation mechanism is different from millimeter-sized droplets. That is, the fluid

transportation at the macroscale does not require the entire droplet to bounce off surfaces due to the existence of breakup which allows a part of droplet to be tossed away; however, owing to the enhanced viscous dissipation at the nanoscale, the breakup could not take place and the only way to achieve the fluid transportation is to induce the bouncing on wettability-controlled surfaces. Therefore, instead of breakup or not, the outcome of nanodroplets impacting wettability-controlled surfaces is classified by whether the bouncing takes place. Because the precondition of fluid transportation at the nanoscale is the bouncing of nanodroplets, before examining the efficient conditions for good performance of fluid transportation, the phase diagram of nanodroplets impacting on surfaces is plotted for distinguishing the cases that nanodroplets can bounce off surfaces, as shown in Fig. 7a. It could be seen that the nanodroplets on surfaces with $\theta_1$ equaling 85°; whereas, with the increases of $\theta_1$ and $\theta_2$, the nanodroplets can bounce off surfaces and the critical impact Weber number decreases simultaneously. Here, a criterion of bouncing is desired to be proposed. As reported by Sanjay et al. (2022), the bouncing transition can be estimated by a function of Bo and Oh. Unfortunately, this criterion is not able to be valid for nanodroplets, because of the small scale of nanodroplets rendering Bo ignorable and the existence of the scale effects. Recently, Ma et al. (2021) investigated the bouncing dynamics of water nanodroplets impact on uniform solid surfaces with $\theta$ and indicated that the bouncing of nanodroplets is more difficult due to the enhanced viscous dissipation. For example, millimeter-sized droplets can bounce off surfaces when $\theta = 90°$ (Mao et al. 1997), whereas, nanodroplets never bounce off surfaces when $\theta < 110°$ regardless of We. At the nanoscale, Ma et al. proposed a criterion of bouncing by considering the balance between the adhesion and the recovered kinetic energy from the maximum spreading state, expressed as $We_{cr} = b\cos\theta + c$, where $b = 162$ and $c = 153$. For using this criterion, the effect of $\theta_1$ and $\theta_2$ is unified to a uniform parameter by $\cos\theta_{uni} = f_1\cos\theta_1 + f_2\cos\theta_2$, where $f_1 + f_2 = 1$. Due to the equal area of the substrates with $\theta_1$ and $\theta_2$, $f_1 = f_2 = 0.5$. Subsequently, Fig. 7a is modified to a $We \sim \theta_{uni}$ phase diagram, as shown in Fig. 7b. Fortunately, by using the uniform contact angle, the criterion can also be valid for bouncing nanodroplets on wettability-controlled surfaces. However, the fitting parameters are shifted to $b = 230$ and $c = 220$. That is, at the same contact angle, the critical Weber number on wettability-controlled surfaces is larger than the one on uniform surfaces, which shows that the wettability-controlled further enhances the viscous dissipation of nanodroplet impacts.

### 3.4 The transportation (lateral) velocity of the bouncing droplet

It is worth noting that, a nanodroplet with a higher impact velocity would have a larger maximum spreading diameter indicating larger surface energy at the maximum spreading state and hence a larger value of transportation velocity if the surface feature is fixed. Therefore, to be fair, the ability of fluid transportation is reasonable to be normalized as $V_t/V_0$. Here needs to emphasize that, due to the enhanced viscous dissipation, $V_t/V_0$ of all nanodroplets tested in this current work does not exceed 0.1 which is significantly lower than the value of 0.23 for millimeter-sized droplets, showing the enhanced viscous dissipation significantly decrease the fluid transportation at the nanoscale. As shown in Fig. 8, $V_t/V_0$ decreases with We increasing and there are two high-efficient fluid transportation regions (distinguished by $V_x/V_0 > 0.05$). (1) As exhibited by the first point on the curves of 125°/180° and 148°/180°, We is required to be as

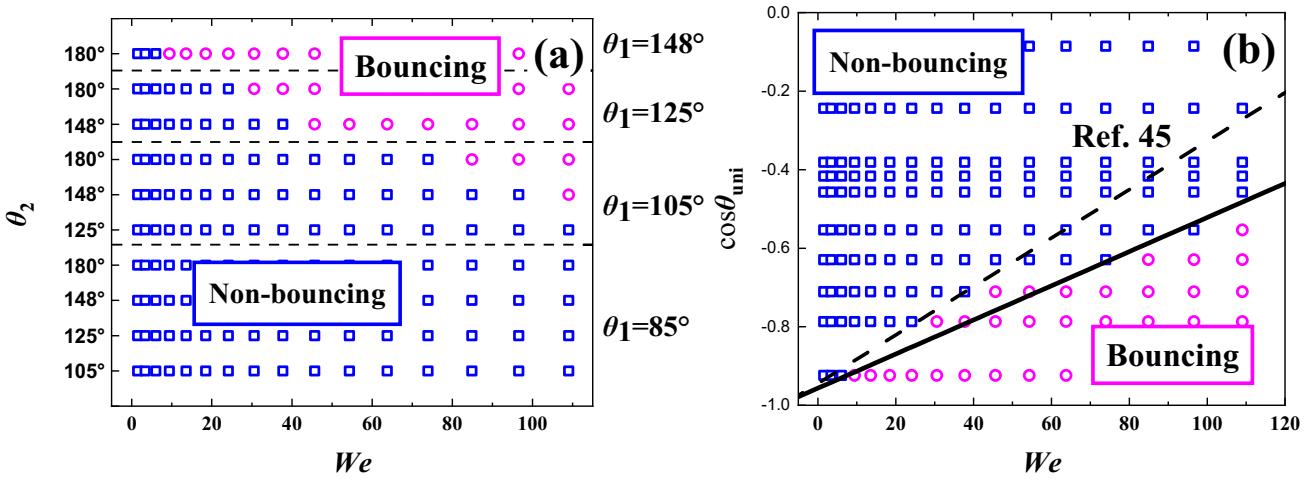


**Fig. 7** **a** $We \sim (\theta_1, \theta_2)$ and **b** $We \sim \cos\theta_{uni}$ phase diagrams of nanodroplets impacting surfaces with different surface wettability and Weber numbers, where $\cos\theta_{uni} = 0.5\cos\theta_1 + 0.5\cos\theta_2$

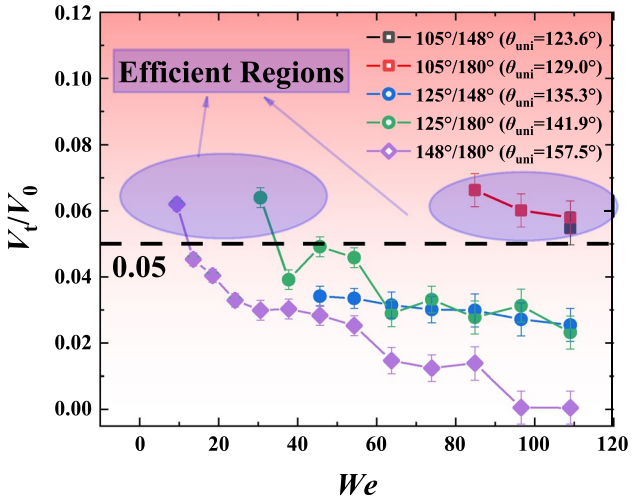


**Fig. 8** Dimensionless lateral velocity $V_t/V_0$ varying with We on surfaces with 105°/148° ($\theta_{uni}$ = 123.6°), 105°/180° ($\theta_{uni}$ = 129.0°), 125°/148° ($\theta_{uni}$ = 135.3°), 125°/180° ($\theta_{uni}$ = 141.9°) and 148°/180° ($\theta_{uni}$ = 157.5°)

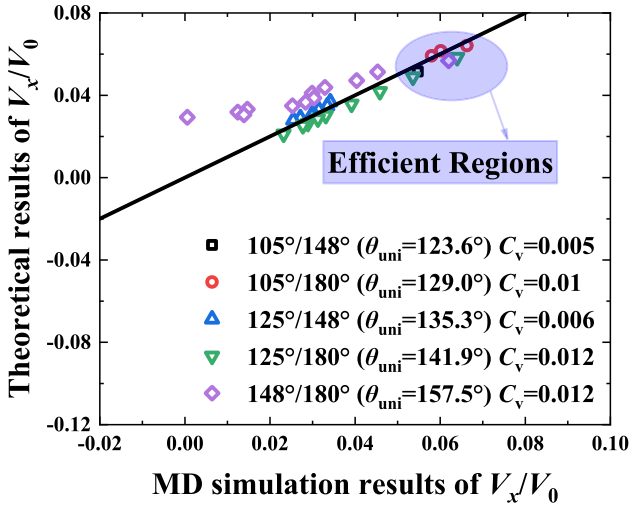


**Fig. 9** The comparison between theoretical results and MD simulations results on wettability-controlled surfaces

low as possible and $\theta_1$ and $\theta_2$ should be as hydrophobic as possible, refer to as the low $\Delta\theta$ region. (2) As exhibited by points of 105°/148° and 105°/180°, $\theta_1$ and $\theta_2$ should be as hydrophilic and hydrophobic as possible, respectively, indicating the high $\Delta\theta$ region for cases where nanodroplets can bounce from surfaces. Obviously, these two regions must correspond to different mechanisms for achieving good performance. Therefore, an energy analysis is implemented for discussing differences for fluid transportation of droplets at the low and high $\Delta\theta$ regions.

A simple energy analysis is implemented for theoretically evaluating the lateral velocity ($V_t$). After a nanodroplet reaches the maximum spreading state, the part of the nanodroplet on the low-wettability side can release more surface energy to kinetic energy during retraction owing to the lower adhesion in comparison with the part on the high-wettability side. Therefore, the transportation velocity stems from the different solid–liquid interfacial energy at different sides of nanodroplets at the maximum spreading state. Here, an energy conservation equation from the maximum spreading state to the bouncing state without viscous effect could be expressed as, $\pi {D_{max}}^2(\cos\theta_1 - \cos\theta_2)/8 = \rho\pi {D_0}^3 {V_t}^2/6$. It is worth noting that, this expression is an inaccurate form owing to significantly viscous dissipation at the nanoscale. For further considering the effect of viscous dissipation in this conservation, an available energy factor, $C_v$ is introduced in the expression as,

$$C_v\left[\frac{1}{8}\pi D_{max}^2(\cos\theta_1 - \cos\theta_2)\right] = \frac{1}{6}\rho D_0^3 V_x^2 \quad (2)$$

As reported by Wang et al. (2020a) that viscous dissipation at the nanoscale is sensitive to surface wettability, $C_v$ must vary with surface features. Here, $C_v$ is an empirical and adjustable parameter to fit different surface features in our simulation system. As shown in Fig. 9, with the wettability decreases, $C_v$ increases from 0.006 to 0.012, indicating the reduction of viscous dissipation. The value of $C_v$ is close to the one on homogeneous and superhydrophobic surfaces as 0.014 reported by Xie et al. (2020). By comparing the prefactor $C_v$ on different wettability-controlled surfaces, it could be seen that the viscous dissipation is violent when $\theta_{uni}$ is low but has a trend of decrease when $\theta_{uni}$ increases. The different solid–liquid interfacial energy at different sides of nanodroplets at the maximum spreading state drives the lateral transportation, however, the viscous dissipation quantified by $C_v$ hinders it. Comparing the different solid–liquid interfacial energy and the viscous dissipation on different wettability-controlled surfaces, the mechanisms of the two high-effective fluid transportation regions become clear. For the low $\Delta\theta$ region, the difference of the solid–liquid interfacial energy is small but the viscous dissipation is low so that a larger proportion of the interfacial energy can convert to transportation kinetic energy; whereas, for the high $\Delta\theta$ region, despite larger viscous dissipation, a larger difference in surface wettability leads to larger difference value of the solid–liquid interfacial energy for proving fluid transportation.

## 4 Conclusions

This work investigated the fluid transportation by droplets impacting wettability-controlled surfaces at the nanoscale via MD simulations. Four kinds of wettability-controlled surfaces, hydrophilic/hydrophobic, hydrophilic/

superhydrophobic, hydrophobic/hydrophobic, and hydrophobic/superhydrophobic, are examined. Our simulation results indicated, although the hydrophilic/superhydrophobic surface can transport droplets with a large distance being about ten times of droplets at the macroscale, such a surface totally falls at the nanoscale because the breakup occurring for millimeter-sized droplets do not take place at the nanoscale during the tossing process, which can be attributed to the entranced viscous dissipation at the nanoscale. Then, fluid transportation is found to be achieved on hydrophobic/hydrophobic and hydrophobic/superhydrophobic surfaces by bouncing nanodroplets instead of breakup. However, there is a contradiction that a more hydrophobic surface is bouncing easier, but is fluid transportation less effective. For identifying what kinds of surface features and impact velocities can show good performance of fluid transportation at the nanoscale, the normalized transportation velocity is extracted by MD simulations, indicating two high-effective fluid transportation regions. One is a low-velocity impact on surfaces with a surface as hydrophobic as possible; the other is a high-velocity impact on surfaces with large $\Delta\theta$. By establishing an energy conservation equation from the maximum spreading state to the bouncing state, the mechanism of these two highly effective regions can be explained by the competition of viscous dissipation and the difference of the solid–liquid interfacial energy. For the former, the viscous dissipation is low for leading to high-effective fluid transportation; whereas, the latter achieves high transportation velocity with the help of a large difference in the solid–liquid interfacial energy.

**Acknowledgements** I would like to express my deep gratitude to Xiao-Dong Wang of NCEPU, for providing the necessary support.

**Funding** This research did not receive any specific grant from funding agencies in the public, commercial, or not-for-profit sectors.

## Declarations

**Conflict of interest** The authors declare that they have no conflict of interests.

## References

Bertola V (2009) An experimental study of bouncing Leidenfrost drops: comparison between Newtonian and viscoelastic liquids. Int J Heat Mass Transf 52:1786–1793

Bird JC, Dhiman R, Kwon H-M, Varanasi KK (2013) Reducing the contact time of a bouncing drop. Nature 503:385–388

Caviezel D, Narayanan C, Lakehal D (2008) Adherence and bouncing of liquid droplets impacting on dry surfaces. Microfluid Nanofluid 5:469–478

Chantelot P, Moqaddam AM, Gauthier A, Chikatamarla SS, Clanet C, Karlin IV, Quéré D (2018) Water ring-bouncing on repellent singularities. Soft Matter 14:2227–2233

Chen L, Li Z (2010) Bouncing droplets on nonsuperhydrophobic surfaces. Phys Rev E Stat Nonlinear Soft Matter Phys 82:016308

Chu F, Luo J, Hao C, Zhang J, Wu X, Wen D (2020) Directional transportation of impacting droplets on wettability-controlled surfaces. Langmuir 36:5855–5862

Galliker P, Schneider J, Eghlidi H, Kress S, Sandoghdar V, Poulikakos D (2012) Direct printing of nanostructures by electrostatic autofocussing of ink nanodroplets. Nat Commun 3:890

Gao S, Liao Q, Liu W, Liu ZJL (2018) Nanodroplets impact on rough surfaces: a simulation and theoretical study. Langmuir 34:5910–5917

Garajeu M, Gouin H, Saccomandi G (2013) Scaling Navier–Stokes equation in nanotubes. Phys Fluids 25:082003

Gilet T, Bush JWM (2012) Droplets bouncing on a wet, inclined surface. Phys Fluids 24:122103

Glasscott MW, Pendergast AD, Goines S, Bishop AR, Hoang AT, Renault C, Dick JE (2019) Electrosynthesis of high-entropy metallic glass nanoparticles for designer, multi-functional electrocatalysis. Nat Commun 10:2650

Gomaa H, Tembely M, Esmail N, Dolatabadi A (2020) Bouncing of cloud-sized microdroplets on superhydrophobic surfaces. Phys Fluids 32:122118

Hao C, Li J, Liu Y, Zhou X, Liu Y, Liu R, Che L, Zhou W, Sun D, Li L, Xu L, Wang Z (2015) Superhydrophobic-like tunable droplet bouncing on slippery liquid interfaces. Nat Commun 6:7986

Hao T, Wang K, Chen Y, Ma X, Lan Z, Bai T (2018) Multiple bounces and oscillatory movement of a microdroplet in superhydrophobic minichannels. Ind Eng Chem Res 57:4452–4461

Hassan G, Yilbas BS, Al-Sharafi A, Sahin AZ, Al-Qahtani H (2020) Solar energy harvesting and self-cleaning of surfaces by an impacting water droplet. Int J Energy Res 44:388–401

Jacobson LC, Kirby RM, Molinero V (2014) How short is too short for the interactions of a water potential? Exploring the parameter space of a coarse-grained water model using uncertainty quantification. J Phys Chem B 118:8190–8202

Josserand C, Thoroddsen ST (2016) Drop impact on a solid surface. Annu Rev Fluid Mech 48:365–391

Jung YC, Bhushan B (2008) Dynamic effects of bouncing water droplets on superhydrophobic surfaces. Langmuir 24:6262–6269

Kobayashi K, Konno K, Yaguchi H, Fujii H, Sanada T, Watanabe M (2016) Early stage of nanodroplet impact on solid wall. Phys Fluids 28:032002

Koishi T, Yasuoka K, Zeng XC (2017) Molecular dynamics simulation of water nanodroplet bounce back from flat and nanopillared surface. Langmuir 33:10184–10192

Kreder MJ, Alvarenga J, Kim P, Aizenberg J (2016) Design of anti-icing surfaces: smooth, textured or slippery? Nat Rev Mater 1:15003

Li X-H, Zhang X-X, Chen M (2015) Estimation of viscous dissipation in nanodroplet impact and spreading. Phys Fluids 27:052007

Li BX, Li XH, Chen M (2017) Spreading and breakup of nanodroplet impinging on surface. Phys Fluids 29:012003

Liu Y, Moevius L, Xu X, Qian T, Yeomans JM, Wang Z (2014) Pancake bouncing on superhydrophobic surfaces. Nat Phys 10:515–519

Ma Q, Wang Y-F, Wang Y-B, He X, Zheng S-F, Yang Y-R, Wang X-D, Lee D-J (2021) Phase diagram for nanodroplet impact on solid surfaces. Phys Fluids 33:102007

Mao T, Kuhn DC, Tran H (1997) Spread and rebound of liquid droplets upon impact on flat surfaces. AIChE J 43:2169–2179

Mishchenko L, Hatton B, Bahadur V, Taylor JA, Krupenkin T, Aizenberg J (2010) Design of ice-free nanostructured surfaces based on repulsion of impacting water droplets. ACS Nano 4:7699–7707

Molinero V, Moore EB (2009) Water modeled as an intermediate element between carbon and silicon. J Phys Chem B 113:4008–4016

Moore EB, Molinero V (2011) Structural transformation in supercooled water controls the crystallization rate of ice. Nature 479:506–508

Okumura K, Chevy F, Richard D, Quéré D, Clanet C (2003) Water spring: a model for bouncing drops. Europhys Lett 62:237–243
Pak CY, Li W, Steve Tse Y-L (2018) Free energy and dynamics of water droplet coalescence. J Phys Chem C 122:22975–22984
Richard D, Quéré D (2000) Bouncing water drops. Europhys Lett 50:769–775
Richard D, Clanet C, Quéré D (2002) Contact time of a bouncing drop. Nature 417:811
Sanjay V, Chantelot P, Lohse D (2022) When does an impacting drop stop bouncing? arXiv preprint arXiv:2208.05935
Schutzius TM, Graeber G, Elsharkawy M, Oreluk J, Megaridis CM (2014) Morphing and vectoring impacting droplets by means of wettability-engineered surfaces. Sci Rep 4:1–7
Sun L, Pan J, Wang X, Jing DJ (2022) Molecular dynamics study of nanoscale droplets impacting on textured substrates of variable wettability. Phys Fluids 34:012005
Wang X, Zeng J, Yu X, Zhang Y (2019a) Superamphiphobic coatings with polymer-wrapped particles: enhancing water harvesting. J Mater Chem A 7:5426–5433
Wang H, Liu C, Zhan H, Liu Y (2019b) Droplet asymmetric bouncing on inclined superhydrophobic surfaces. ACS Omega 4:12238–12243
Wang YB, Wang XD, Yang YR, Chen M (2019c) The maximum spreading factor for polymer nanodroplets impacting a hydrophobic solid surface. J Phys Chem C 123:12841–12850
Wang YB, Wang YF, Gao SR, Yang YR, Wang XD, Chen M (2020a) Universal model for the maximum spreading factor of impacting nanodroplets: from hydrophilic to hydrophobic surfaces. Langmuir 36:9306–9316
Wang YF, Wang YB, Xie FF, Liu JY, Wang SL, Yang YR, Gao SR, Wang XD (2020b) Spreading and retraction kinetics for impact of nanodroplets on hydrophobic surfaces. Phys Fluids 32:092005
Wang J, Lang T, Liu H, Chen Y, Li L, Liu Y, Zhu W (2022) Improved output force response speed of the biological gel artificial muscle prepared from carboxylated chitosan and sodium carboxymethyl cellulose. Mech Adv Mater. https://doi.org/10.1080/15376494.2022.2035024
Xie FF, Lu G, Wang XD, Wang BB (2018a) Coalescence-induced jumping of two unequal-sized nanodroplets. Langmuir 34:2734–2740
Xie FF, Lu G, Wang XD, Wang DQ (2018b) Enhancement of coalescence-induced nanodroplet jumping on superhydrophobic surfaces. Langmuir 34:11195–11203
Xie FF, Lv SH, Yang YR, Wang XD (2020) Contact time of a bouncing nanodroplet. J Phys Chem Lett 11:2818–2823
Zhang B-X, Wang S-L, Wang X-D (2019) Wetting Transition from the Cassie–Baxter state to the Wenzel state on regularly nanostructured surfaces induced by an electric field. Langmuir 35:662–670
Zhang BX, Wang SL, Wang YB, Yang YR, Wang XD, Yang RG (2021) Harnessing reversible wetting transition to sweep contaminated superhydrophobic surfaces. Langmuir 37:3929–3938